JOURNAL OF SPACECRAFT AND ROCKETS
Vol. 43, No. 3, May–June 2006

Micronewton Thruster Requirements for Earth-Orbiting Imaging Formations

J. J. Blandino* and B. St. Rock†
Worcester Polytechnic Institute, Worcester, Massachusetts 01609

Previous studies have explored options for separated spacecraft interferometers for planet detection as well as optical imaging of astrophysical objects. As others have noted, one of the benefits of Earth-orbiting formations is the potential to reduce the propellant required to complete image (u–v) plane filling maneuvers by taking advantage of gravity-gradient forces. In this work, the equations of motion for each of the three spacecraft in a linear formation are numerically integrated using an acceleration profile previously proposed by DeCou to produce a gradual filling of the image plane. The analysis also includes the addition of the J_2 perturbing acceleration and provides the detailed spacecraft position, velocity, and thrust histories for a maneuver as well as the maximum baseline rate of change and ΔV. Results suggest that micronewton thrusters under development for other missions requiring precision spacecraft control might be enabling for the Earth-orbiting imaging formation considered here. For one of the reference cases in geostationary orbit with a maximum baseline of 1 km and an allocated maneuver time of five days, the maximum thrust and throttling rate are approximately 87 μN and 0.24 μN/min, respectively, with a maximum baseline rate of change of 2.4 cm/s and ΔV of 6 cm/s for a single maneuver (one observation). The same reference case with thruster cancellation of the J_2 acceleration results in a maximum thrust of 2.1 mN and ΔV of 3.6 m/s. The maximum thrust, baseline rate of change, and ΔV are presented for maneuver times of one to five days, maximum baselines of 250 m and 1 km, and a formation altitude of 35,786 and 20,000 km. Three propulsion technology options—pulsed plasma, field emission electric propulsion, and colloid—are discussed as possible candidates for this role. Two solution strategies are proposed to the problem raised by the J_2 perturbation.

Nomenclature

$\boldsymbol{a}_p$	=	J_2 acceleration in the geocentric equatorial system, m/s^2
a_{r_0}	=	initial radial acceleration in u–v imaging plane, m/s^2
$\boldsymbol{a}_t$	=	thrust acceleration in u–v imaging plane, m/s^2
$D_{\max}$	=	maximum interferometer baseline, m
D_0	=	initial formation baseline, m
$g(t)$	=	spiral path function during plane filling maneuver, m
g_0	=	initial distance between collector and combiner spacecraft in u–v plane, m
$\hat{\boldsymbol{I}}, \hat{\boldsymbol{J}}, \hat{\boldsymbol{K}}$	=	unit vectors for geocentric equatorial coordinate system
$\hat{\boldsymbol{i}}, \hat{\boldsymbol{j}}, \hat{\boldsymbol{k}}$	=	unit vectors for formation-centered coordinate system
J_2	=	second-order zonal harmonic coefficient
m_{coll}	=	mass of each collector spacecraft, kg
$R_\oplus$	=	Earth's radius, m
$\boldsymbol{r}$	=	Cartesian position vector in geocentric equatorial coordinate system, m
$\boldsymbol{S}$	=	state vector in geocentric equatorial coordinate system
T_{ijk}	=	transformation matrix from geocentric to formation-centered coordinate system
t_{fill}	=	time required to fill the u–v imaging plane, s
v_{r_0}	=	initial radial velocity in u–v imaging plane, m/s
x, y, z	=	Cartesian components of position vector in geocentric equatorial system, m
μ	=	gravitational parameter, m^3/s^2
τ	=	time allocated for completion of plane filling maneuver, s
ϕ, ψ	=	Euler angles used to orient formation-centered coordinate system with target, deg
ω	=	angular frequency of circular orbit at a given altitude, rad/s

Received 29 December 2004; revision received 20 July 2005; accepted for publication 22 July 2005.

*Assistant Professor, Mechanical Engineering Department. Senior Member AIAA.
†Graduate Student, Mechanical Engineering Department. Student Member AIAA.

I. Introduction

THE use of three spacecraft flying in an Earth-trailing heliocentric trajectory was studied extensively as part of NASA New Millennium Program's former Deep Space 3 (DS-3) mission. In the original mission concept, three spacecraft were to fly in formation in a triangle in which two "collector" spacecraft, forming the base of the triangle, collect starlight and redirect it in a collimated beam to a "combiner" spacecraft forming the apex of the triangle. These beams are combined to form interference fringes that provide information about the brightness distribution for the astrophysical target.[1] This information is collected at a number of discrete points in the image (or u–v) plane. The u–v plane is perpendicular to the line of sight between the combiner spacecraft and the target star. The interferometer baseline for an observation corresponds to the component of the vector separating the two collector spacecraft that lies in the u–v plane. Observing a particular object then involves observing fringes at different baselines and baseline orientations in inertial space. The number of specific points will depend on the desired resolution and complexity of the object.[1]

In the original DS-3 studies, the approach adopted for filling the synthetic aperture (u–v) plane was referred to as "stop and stare," so named because the collector spacecraft were brought to rest relative to each other in inertial space during the collection of data. The elimination of relative spacecraft velocity between points and the need to move to many different points was propulsion intensive for a mission in which many objects were to be imaged with a high density of points in the u–v plane.[2]

Before the studies for DS-3, DeCou[3,4] had proposed a strategy for u–v plane filling in which the gravity gradient between two spacecraft in slightly different orbits around a central spacecraft in geostationary orbit was used to provide a means of continuously varying the observation baseline of the formation over several orbits with minimal propulsion. In the context of formation flying, the gravity gradient refers to the differential gravitational acceleration

between the three spacecraft caused by their relative separation. This "orbit evolution observing mode" was also investigated by Linfield (documented in Linfield, R., "DS3 in Geosynchronous Orbit: A First Look at Orbital Dynamics, u–v Coverage, and Detection Thresholds," Jet Propulsion Laboratory, Interoffice Memorandum No. 335.1-98-003, Pasadena, CA, 31 March 1998) as part of a DS-3 mission study evaluating the potential advantages of a geostationary DS-3 mission. Among other issues, Linfield evaluated the implications of the orbit evolution observing mode on specific instrument requirements and detection sensitivity.

The thrust required for the continuous plane filling approach developed by DeCou scales linearly with spacecraft mass. In his original work he assumed a spacecraft mass comparable with the Hubble Space Telescope ($\approx 10^4$ kg). Work associated with the DS-3 mission suggests about an order-of-magnitude lower mass for a viable spacecraft interferometer, a difference that has significant implications for the choice of propulsion system. In addition to the pulsed plasma thrusters (PPT) considered in the DS-3 studies, the development of micronewton thrusters such as colloid and field emission thrusters in the last several years for missions such as ST-7 and Laser Interferometer Space Antenna (LISA) have broadened the technology options for precision formation control. These technologies expand the mission designer's options beyond the PPT and cold-gas systems previously considered.

The plane filling approach described by DeCou assumes that data are collected while the spacecraft have a velocity relative to each other. If a laser metrology system[5] is used to determine relative spacecraft positions, the presence of a relative velocity imposes demanding sampling rate requirements as described by Linfield. A second, related issue results from differential velocities of the collector spacecraft relative to the combiner. Such differential velocities introduce the need for the instrument "delay line" to compensate for the differences in the starlight path length (delay) and the rate of change of this path length (delay rate). Saturation of the delay line will require an interruption in the observation, whereas the relative spacecraft velocity will have implications for both delay rate and metrology system sampling rate as just mentioned. Both of these issues were considered by Linfield. As a result of these instrument limitations, the present analysis also evaluates this baseline rate of change as a key performance metric.

In summary, given the progress in definition of spacecraft and instruments for an imaging formation, as well as the continued development of micronewton thrusters since DeCou's description of this formation in 1991, the present study was undertaken to further evaluate detailed propulsion requirements for that formation. The work presented in this paper significantly extends DeCou's analytical results by including zonal harmonic J_2 acceleration in the force model used for orbit propagation. Specifically, this work will 1) update some of the findings in Ref. 3 by using more current estimates for the collector spacecraft mass; 2) examine the validity of the earlier analytical results by numerically solving the equations of motion for each of the three spacecraft with the inclusion of J_2 perturbations; 3) evaluate the maximum baseline rate of change, which has important implications for metrology system sampling rates; 4) evaluate sensitivity of the maximum required thrust, ΔV and baseline rate of change to orbital altitude, allocated time for the plane filling maneuver, and maximum interferometer baseline; and 5) describe three propulsion technologies that we consider enabling for such a mission. This work extends a previous effort considering DeCou's formation in which his analytical results were used to explore some of the micronewton level thrust requirements.[6]

This paper is organized as follows: in Sec. II, we describe the formation originally proposed by DeCou and the coordinate systems used in the analysis. This is followed in Sec. III by a description of the numerical solution of the equations of motion used to propagate the orbits for the three spacecraft. Detailed results are then presented in Sec. IV for two reference cases. These results include reporting the velocity and thrust histories, spacecraft relative motion paths in the u–v plane, as well as the rate of change of the aperture baseline for an entire plane filling operation. The sensitivities of the maximum required thrust, required ΔV, and baseline rate of change to time allocated to plane filling, orbital altitude, and maximum baseline are also presented. The implications of the J_2 perturbation are also discussed in Sec. IV. Sec. V describes three propulsion technologies that have matured significantly in the last decade and that we consider enabling for this mission. In Sec. VI, the propulsion options are revisited in light of the calculated requirements, including two proposed solutions to the problem raised by the J_2 perturbations. Conclusions are presented in Sec. VII.

II. Spacecraft Formation

A. Reference Frames

The geosynchronous formation originally proposed by DeCou[3] consists of three satellites in a linear arrangement. The center satellite, which in this paper will be designated the "combiner," remains in a zero inclination orbit and is located midway between the two outer, or "collector" spacecraft. Each of the collector spacecraft have equal orbital inclination but have a right ascension of the ascending node, which are 180 deg apart. The argument of perigee and true anomaly is set such that the three spacecraft form a close formation, with a relative separation determined by the baseline of the formation. As a result of this differential element set, the collector spacecraft are always on opposite sides of the combiner orbital plane (which corresponds to the Earth's equatorial plane). In general, each collector orbit will differ from that of the combiner by an equal amount of inclination (on the order of 10^{-6} deg for the cases considered here), but they will constantly remain in opposite hemispheres because of the offset in their right ascensions. Because the two collector spacecraft are in slightly different orbits, they will be subject to a relative gravity-gradient acceleration. This relative acceleration is fully described in an earlier work by DeCou investigating disturbances on rotating tethered systems in circular Earth orbit.[4]

The present analysis is described with respect to two nonrotating coordinate systems as in Ref. 3. These two reference frames are shown in Fig. 1. The first is a geocentric equatorial system designated by IJK in which the $\hat{\boldsymbol{I}}$ vector points in the direction of the vernal equinox, the $\hat{\boldsymbol{K}}$ vector coincides with the Earth's rotational axis, and the $\hat{\boldsymbol{J}}$ vector completes an orthogonal set. This reference frame is used primarily to define the Cartesian vectors used in the numerical propagation of the orbits but is also convenient to describe the location of astronomical targets in the sky as well as the orbital elements for the spacecraft.

The second coordinate system, designated by ijk, is a nonrotating frame centered on the combiner spacecraft with the $\hat{\boldsymbol{k}}$ unit vector pointing towards the astronomical source object. The $\hat{\boldsymbol{i}}$ and $\hat{\boldsymbol{j}}$ vectors are orthogonal to $\hat{\boldsymbol{k}}$ and define that object's u–v plane. The coordinate transformation between the Earth-centered IJK and formation-centered ijk coordinate systems involves two successive rotations.

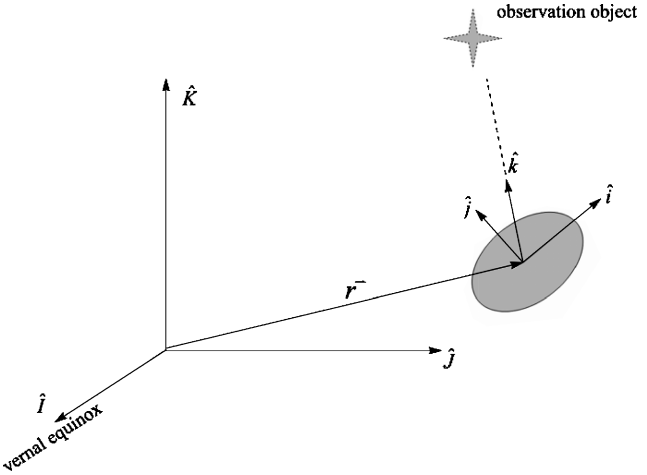

Fig. 1 Coordinate systems referenced. The u–v imaging plane lies in the formation-centered ijk coordinate system. The $\hat{k}$ unit vector points along the line of sight to the target object. The position vector r lies in the Earth's equatorial $\hat{I}\hat{J}$ plane.

The first rotation is through an angle ψ about the K axis. If the intermediate system defined by this first rotation has axes designated by $I'J'K'$, a second rotation through an angle ϕ about the J' axis completes the transformation to the ijk system. The angles ψ and ϕ correspond to the geocentric right ascension and (90 deg minus) the declination respectively. These two angles define the target star's coordinates in the sky and determine how the $\hat{\boldsymbol{i}}$ and $\hat{\boldsymbol{j}}$ vectors will be oriented in the u–v plane. These two rotations define a transformation matrix T_{ijk} to convert from the Earth-centered IJK and formation-centered ijk coordinate systems:

$$T_{ijk} = \begin{bmatrix} \cos(\psi)\cos(\phi) & \sin(\psi)\cos(\phi) & -\sin(\phi) \\ -\sin(\psi) & \cos(\psi) & 0 \\ \cos(\psi)\sin(\phi) & \sin(\psi)\sin(\phi) & \cos(\phi) \end{bmatrix} \tag{1}$$

The transpose of this matrix provides the transformation back to the IJK system.

B. Spacecraft Path in Imaging Plane

The collector spacecraft are positioned symmetrically on either side of the combiner spacecraft resulting in a linear formation. The path of the collector spacecraft relative to the combiner (at the origin of the ijk system) determines how the u–v plane will be "filled" because observations of the target star would be made along this path. The advantage of DeCou's approach is that the gravity-gradient acceleration results in a periodic motion of the collector that fills in points in the u–v plane while minimizing the need for propulsion.

To minimize the need for interferometer delay line compensation, the path component out of the u–v plane (in the $\hat{\boldsymbol{k}}$ direction) should be zero. In Ref. 3, DeCou shows that this condition can be satisfied for the path of the collector given by

$$\boldsymbol{P}(t) = g(t)\sin(\omega t - \psi)\hat{\boldsymbol{i}} - g(t)\cos\phi\cos(\omega t - \psi)\hat{\boldsymbol{j}} + 0\hat{\boldsymbol{k}} \tag{2}$$

where $\boldsymbol{P}(t)$ is the collector's vector path in time with components $P_1(t)$, $P_2(t)$, and $P_3(t)$ in the ijk coordinate system. In Eq. (2), ω is the angular orbital velocity of the combiner spacecraft at the altitude of interest, and $g(t)$ is an arbitrary function of time. The ratio of the minor to major axis for the ellipse followed in the u–v plane is given in terms of the target Euler angle through the $\cos\phi$ term. DeCou demonstrates analytically that the path described by Eq. (2), where $g(t)$ is an arbitrary function, satisfies the requirement that the majority of acceleration needed is provided by the gravity-gradient acceleration with an out-of-plane $\hat{\boldsymbol{k}}$ component, which remains zero. He goes on to derive an expression for the acceleration required by the thrusters, also specified in terms of the path function $g(t)$. This thruster acceleration is

$$\boldsymbol{a}_t = \begin{bmatrix} 2g'(t)\omega\cos(\omega t - \psi) + g''(t)\sin(\omega t - \psi) \\ \cos\phi[2g'(t)\omega\sin(\omega t - \psi) - g''(t)\sin(\omega t - \psi)] \\ 0 \end{bmatrix} \tag{3}$$

If $g(t)$ is a constant (no thrusting), then each collector would complete an elliptical path in the u–v plane every orbit. Reference 3 considers the case with $g(t)$ corresponding to a linearly increasing function of time.

In this work, the equations of motion for each of the three spacecraft are integrated numerically, as described in the next section, using the initial state defined by Eq. (2), its derivative, and a thrust acceleration profile prescribed by Eq. (3). Rather than using a path function that is linearly increasing in time, we consider the case where each collector begins and ends its plane filling maneuver with no thrusting. This would be the case if the spacecraft are following their natural orbits, tracing an ellipse in the u–v plane as specified by Eq. (2) with $g(t)$ equal to a constant. When the thrusters are turned on, a radial acceleration is produced in the u–v plane such that the plane filling begins. The collectors accelerate radially outward for a prescribed period of time and then begin to decelerate such that they trace a new ellipse (with no thrusting) at the end of the maneuver. To achieve this motion, the general expression used in this work for the path function $g(t)$ is given by

$$g(t) = g_0 + v_{r_0}t + \tfrac{1}{2}a_{r_0}t^2 \tag{4}$$

where g_0, v_{r_0}, and a_{r_0} represent the initial spiral radial position, velocity, and acceleration in the u–v plane. The analysis presented in Ref. 3 considered the case with no radial acceleration and constant radial velocity ($v_{r_0} \neq 0$, $a_{r_0} = 0$). Because we assume the thrusters transition between plane filling maneuvers with a period of no thrusting, the spiral begins with an initial position given by g_0 and no initial radial velocity $v_{r_0} = 0$. For a maneuver in which the collectors are spiraling outward (increasing baseline), the path acceleration will be given by

$$g''(t) = 0, \qquad t = 0, \qquad g''(t) = a_{r_0}, \qquad 0 < t \leq \tau/2$$
$$g''(t) = -a_{r_0}, \qquad \tau/2 < t \leq \tau \tag{5}$$

where τ is the fill time allocated for the plane filling maneuver, which might or might not be some multiple of the orbital period at the altitude of interest. If the maneuver involves transitioning from a larger to smaller baseline (i.e., closing the ellipse), then the sign of the acceleration would be changed between the first and second half-periods. The preceding profile ensures that the collectors begin and end their plane filling maneuver in a natural orbit, which results in an elliptical path in the u–v plane with no thrusting. We obtain the thrust profile used in the numerical integration of the equations of motion results by using Eq. (5) in thrust acceleration equation (3).

III. Numerical Solution

A. Formation Initialization

Defining the initial conditions for the formation requires specifying an altitude for the combiner, the target object coordinates in terms of the Euler angles ψ and ϕ, and the initial separation g_0 of each collector (assumed to be arranged in a linear, symmetrical formation) from the combiner. The equations of motion (including a thrust acceleration term for the collector spacecraft) are numerically integrated using MATLAB®. Up to this point, we have described the spacecraft paths in terms of the formation ijk coordinate system. The orbit integration however is performed with Cartesian coordinates referenced to the Earth-centered IJK coordinate system. The equations of motion are expressed in a state-variable form for this purpose, which requires a transformation between coordinate systems.

The combiner spacecraft is always in a circular, equatorial orbit (though not necessarily geosynchronous). Differentiating Eqs. (2) and (4) provides expressions for the velocity components in the ijk coordinate system

$$\dot{\boldsymbol{P}}(t) = \begin{bmatrix} g(t)\omega\cos(\omega t - \psi) + g'(t)\sin(\omega t - \psi) \\ g(t)\cos\phi\omega\sin(\omega t - \psi) - g'(t)\cos\phi\cos(\omega t - \psi) \\ 0 \end{bmatrix} \tag{6}$$

The initial position and velocity of the symmetrically arranged collector spacecraft are then found from Eqs. (2) and (6) with $t = 0$.

Defining the state space vector for the ith spacecraft as

$$\boldsymbol{S}_i = \begin{bmatrix} \boldsymbol{r}_i \\ \dot{\boldsymbol{r}}_i \end{bmatrix}$$

the initial state vector for the first collector spacecraft can be expressed in the geocentric equatorial IJK system as

$$\boldsymbol{S}_{\text{coll}_1} = \boldsymbol{S}_{\text{comb}} + \begin{bmatrix} T_{ijk}^T P \\ T_{ijk}^T \dot{P} \end{bmatrix} \tag{7}$$

where we have used the transpose of the coordinate transformation matrix given by Eq. (1) to convert the initial position and velocity from the formation-centered coordinate system. The second collector position and path will be symmetric about the combiner, so that

$$\boldsymbol{S}_{\text{coll}_2} = \boldsymbol{S}_{\text{comb}} - \begin{bmatrix} T_{\text{ijk}}^T P \\ T_{\text{ijk}}^T \dot{P} \end{bmatrix} \tag{8}$$

Together, $\boldsymbol{S}_{\text{coll}_1}$, $\boldsymbol{S}_{\text{coll}_2}$, and $\boldsymbol{S}_{\text{comb}}$ at $t=0$ represent the initial conditions of all three spacecraft in the Earth-centered *IJK* coordinate system.

B. Orbit Propagation

The orbit of the combiner spacecraft is propagated numerically using two-body mechanics. The two-body equation of motion is modified by an additional perturbing acceleration caused by zonal harmonic distributions in the Earth's mass (J_2 effects):

$$\ddot{r} = -(\mu/r^2)(\boldsymbol{r}/r) + \boldsymbol{a}_P \tag{9}$$

For each of the two collector spacecraft, this equation is modified by a thrust acceleration term given by Eq. (3) in the *ijk* system:

$$\ddot{\boldsymbol{r}} = -(\mu/r^2)(\boldsymbol{r}/r) + \boldsymbol{a}_P + T_{\text{ijk}}^T \boldsymbol{a}_t \tag{10}$$

To propagate the orbital motion, the equation of motion is integrated numerically using the ode45 solver in MATLAB. In state-variable form, Eq. (10) for the collector spacecraft can be written as

$$\begin{bmatrix} \dot{x} \\ \dot{y} \\ \dot{z} \\ \ddot{x} \\ \ddot{y} \\ \ddot{z} \end{bmatrix} = \begin{bmatrix} & 0_{3x3} & & I_{3x3} \\ -\mu/r^3 & 0 & 0 & \\ 0 & -\mu/r^3 & 0 & 0_{3x3} \\ 0 & 0 & -\mu/r^3 & \end{bmatrix} \begin{bmatrix} x \\ y \\ z \\ \dot{x} \\ \dot{y} \\ \dot{z} \end{bmatrix} + T_{ijk}^T \begin{bmatrix} 0 \\ 0 \\ 0 \\ a_{t_x} \\ a_{t_y} \\ a_{t_z} \end{bmatrix} + \begin{bmatrix} 0 \\ 0 \\ 0 \\ a_{P_x} \\ a_{P_y} \\ a_{P_z} \end{bmatrix} \tag{11}$$

with $\boldsymbol{r} = x\hat{I} + y\hat{J} + z\hat{K}$, etc. A similar equation (without the thrust acceleration term) is solved for the combiner spacecraft. The last term represents the perturbing acceleration caused by J_2 effects. We use a simplified model by Vallado[7] for the aspherical gravitational potential with zonal acceleration components in the *IJK* coordinate system given by

$$a_{P_x} = -\frac{3J_2\mu R_\oplus^2 x}{2r^5}\left(1 - \frac{5z^2}{r^2}\right)$$

$$a_{P_y} = -\frac{3J_2\mu R_\oplus^2 y}{2r^5}\left(1 - \frac{5z^2}{r^2}\right), \qquad a_{P_z} = -\frac{3J_2\mu R_\oplus^2 z}{2r^5}\left(3 - \frac{5z^2}{r^2}\right) \tag{12}$$

where $J_2 = 0.0010826269$ is the second-order zonal harmonic coefficient.

As noted earlier, a plane filling maneuver consists of applying the thrust profile as specified by Eq. (5) to spiral "out" and increase the interferometer baseline or to spiral "in" and decrease the baseline. A likely mission scenario would involve spiraling out by increasing the baseline and collecting points throughout the u–v plane, then retargeting (changing the angles ψ and ϕ) followed by a spiral in (back to the initial baseline) and thus collecting data for another source.

As a practical matter, for the cases discussed in the following section, the plane filling time τ allowed for the maneuver was selected to be one of the independent variables for the analysis. For this reason, the value for the acceleration a_{r_0} in Eq. (5) was solved iteratively subject to a 0.1-m tolerance on the maximum baseline. Once the maximum baseline is reached within the fill-time constraints given, the acceleration history given by Eq. (3) was multiplied by the spacecraft mass to obtain a thrust history. For the relatively high-specific-impulse propulsion systems under consideration, the spacecraft wet mass change will be negligible even after many plane filling maneuvers to image numerous targets.

IV. Results and Discussion

In this section, the results of the formation analysis are discussed, specifically with respect to their implications for propulsion system options. Section IV.A describes two reference cases that are presented in detail to identify thrust level and modulation requirements, as well as detailed characteristics of the plane filling path. The second subsection presents results characterizing the sensitivity of maximum thrust magnitude, baseline rate, and ΔV to plane filling time, orbital altitude, and final baseline. The range of filling time considered spans one to ten days (five days for the reference cases). In DeCou's analysis he considered maneuver times as long as 50 days; however, given that the observation science time allocated for the DS-3 studies was approximately four months,[1] we have chosen to consider one to five days to allow for a reasonable number of science targets within a period on the order of a few months.

A. Reference Cases

Two reference cases were selected for the purpose of presenting detailed characteristics of the plane filling maneuver. For each of these cases, the combiner spacecraft is located in geosynchronous orbit with the collectors positioned with an initial radial coordinate in the u–v plane g_0 equal to 10 m. The collector spacecraft mass is 250 kg, and the final baseline is 1000 m reached after a fill time equal to five days. The first case corresponds to a target object specified by angular coordinates $\phi = 0$, $\psi = 0$, whereas the second case corresponds to a target with the coordinates $\phi = 45$ deg, $\psi = 0$. The orbital element sets that correspond to these cases are reported in Table 1. Although the angle ψ introduces a phasing in the position [through Eq. (2)] and the thrust modulation [through Eq. (3)], it does not significantly change either the propulsion requirements or characteristics of the plane filling trajectory. The angle ϕ, on the other hand, does have a significant effect on the thrust profile and trajectory. From Eq. (2), for any case with $\psi = 0$, the initial baseline

Table 1 Initial orbital element set of the spacecraft for all cases

Combiner orbit (altitude, km)	ϕ, deg[a]	Spacecraft	a, km	ε	i, deg	Ω, deg	ω, deg	ν, deg
GEO (35,786)	0	Combiner	42,164	0	0	0	0	0
		Collector 1	42,164	8.4429e−14	0	N/A	−1.3607e−5[b]	−1.8017e−8
		Collector 2	42,164	8.4429e−14	0	N/A	1.3607e−5[b]	1.8017e−8
GEO (35,786)	45	Combiner	42,164	0	0	0	0	0
		Collector 1	42,164	7.0367e−14	9.6087e−6	180-Ω_2[c]	180 + ν_2[c]	−3.3434e−8
		Collector 2	42,164	7.0367e−14	9.6087e−6	9.6087e−6	−3.3434e−8	3.3434e−8
MEO (20,000)	45	Combiner	26,378	0	0	0	0	0
		Collector 1	26,378	1.7970e−13	1.5359e−5	180-Ω_2[c]	180 + ν_2[c]	−5.8932e−9
		Collector 2	26,378	1.7970e−13	1.5359e−5	1.5359e−5	−5.8932e−9	5.8932e−9

[a]The geocentric right ascension of all cases is $\psi = 0$.
[b]For the elliptical equatorial case, this element corresponds to the true longitude of periapsis, as defined in Ref. 7.
[c]Subscript 2 refers to the corresponding element of collector 2.

($t = 0$) will be given by

$$D_0 = 2g_0 \cos\phi \tag{13}$$

The first reference case, with $\phi = 0$, corresponds to the case in which the u–v and equatorial planes coincide and the target star line of sight is parallel with the Earth's axis of rotation. For this case, the $\cos\phi$ term appearing in Eq. (2) is equal to unity, and the paths will be a circular spiral, from the initial to the final baseline. From Eq. (12) the initial baseline will be 20 m. The results for this reference case are presented in Figs. 2–6.

The paths of the two collector spacecraft in the u–v plane are shown in Fig. 2. The reader is reminded that the ijk coordinate system has its origin at the combiner spacecraft (and hence the origin of Fig. 2). From Eq. (2), prior to thrust being applied, the two collector spacecraft would trace a circular path around the combiner. Applying a thrust acceleration as prescribed by Eqs. (3–5) results in the spiral trajectory shown, in which the separation of each successive pass increases for the first two and a half days, after which the acceleration is reversed, resulting in paths that are more closely spaced together until the collector has reached the final baseline with negligible radial velocity. If one were to consider a much larger final baseline, say, many tens of kilometers, then a different acceleration

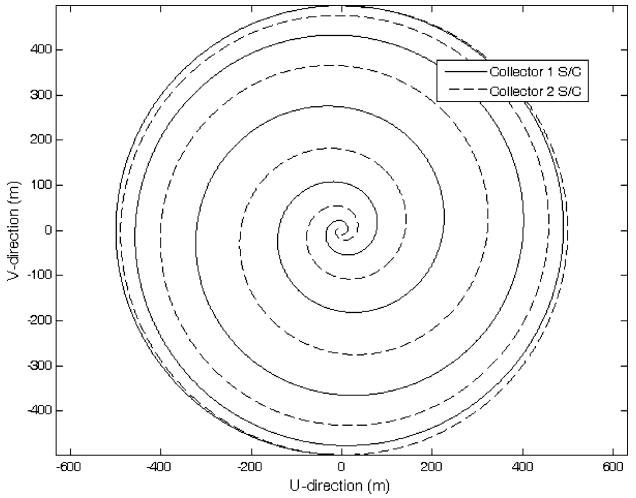

Fig. 2 Path of two collector spacecraft in u–v plane for case corresponding to $D_{\max} = 1000$ m, $\phi = 0$ deg, $\psi = 0$ deg, GEO, and $t_{\text{fill}} =$ five orbits.

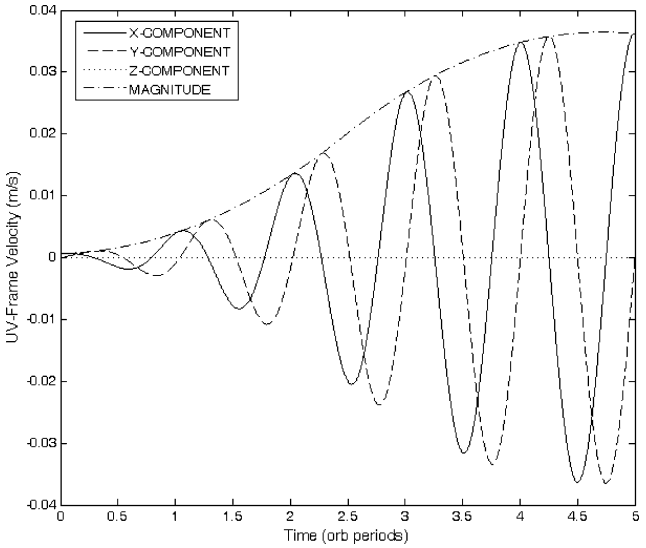

Fig. 3 Velocity components of collector spacecraft in u–v plane for case corresponding to $D_{\max} = 1000$ m, $\phi = 0$ deg, $\psi = 0$ deg, GEO, and $t_{\text{fill}} =$ five orbits.

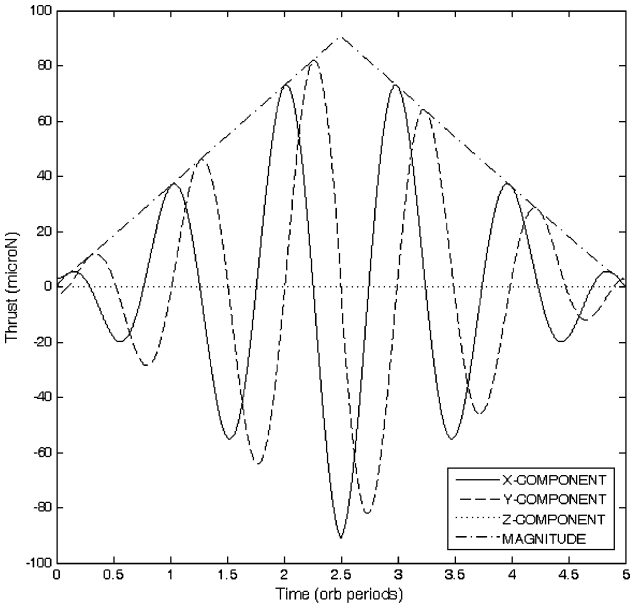

Fig. 4 Thrust components of collector spacecraft in u–v plane for case corresponding to uncompensated J_2 perturbations and $D_{\max} = 1000$ m, $\phi = 0$ deg, $\psi = 0$ deg, GEO, $t_{\text{fill}} =$ five orbits, and $m_{\text{coll}} = 250$ kg.

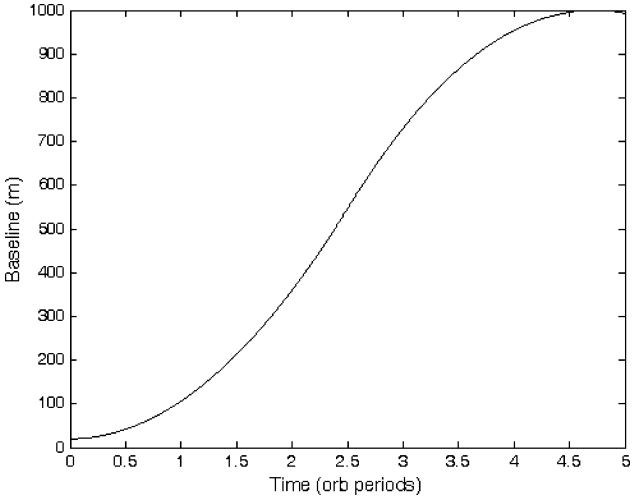

Fig. 5 Formation baseline as a function of time for case corresponding to $D_{\max} = 1000$ m, $\phi = 0$ deg, $\psi = 0$ deg, GEO, and $t_{\text{fill}} =$ five orbits.

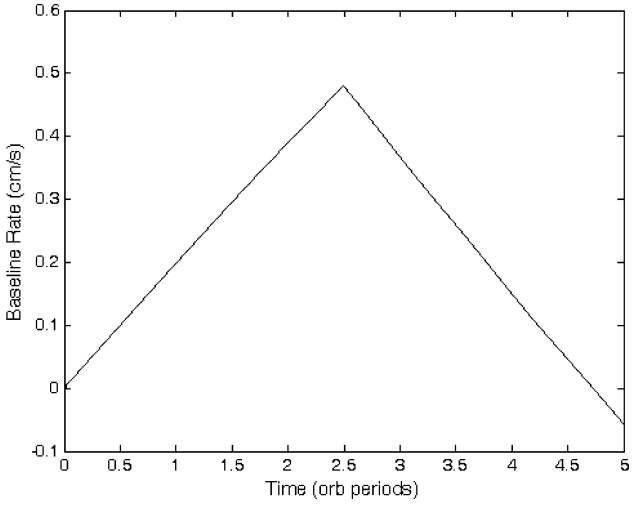

Fig. 6 Formation baseline rate of change as a function of time for case corresponding to $D_{\max} = 1000$ m, $\phi = 0$ deg, $\psi = 0$ deg, GEO, and $t_{\text{fill}} =$ five orbits.

profile from that given by Eq. (5) could be used so as to introduce a "coasting" period such that the spacing between successive passes would remain uniform until a point at which thrusting is reapplied so as to eliminate the relative velocity.

Figure 3 presents the magnitude and components of the velocity in the *ijk* coordinate system. One of the constraints used by DeCou in Ref. 3 to derive the thrust acceleration profile [Eq. (3)] was the absence of any motion out of the image plane ($\hat{\boldsymbol{k}}$ direction). As will be discussed in Sec. V, the J_2 perturbation introduces an out-of-plane drift. In this work the thrust acceleration profile in Eq. (3) is applied and the equations of motion solved. There is no additional constraint to eliminate motion in the $\hat{\boldsymbol{k}}$ direction, but rather the absence of such motion (when the J_2 acceleration is neglected) is used a means of checking the consistency of the solutions.

Figure 4 shows the thrust magnitude and components in the u–v plane corresponding to the case that does not compensate for the out-of-plane motion introduced by J_2. The maximum thrust magnitude is approximately 91 μN. As with all of the results, the fundamental timescale is the orbital period. There is another feature of the required thrust profile that will have an impact on the thruster (and associated control system). From Eqs. (3) and (5), there can be a discontinuity in the one of the components because the radial acceleration a_{r_0} changes sign at $t = \tau/2$. This is evident from close inspection of Fig. 4. At a time equal to 2.5 periods, the collector spacecraft has reached its maximum baseline rate of change and begins to slow this rate down to complete the maneuver (see also Fig. 6). The x component of the thrust has peaked in magnitude at this point, and thus when a_{r_0} changes sign the x component begins to decrease in magnitude. At a time equal to 2.5 periods, the y component is still decreasing however. The change in the sign of a_{r_0} at this point results in a discontinuity in the thrust y component as it changes abruptly from approximately $+3$ to -3 μN. In practice, such a change would be accomplished through switching different thrusters on and off. As will be discussed in Sec. V, the thrusters under consideration can be turned on or off within very short timescales (<100 ms).

As described in the Introduction, the interferometer baseline for an observation corresponds to the component of the vector separating the two collector spacecraft that lies in the u–v plane. Because of the inclusion of J_2 acceleration, an out-of-plane component of motion develops for some of the cases considered. To be conservative in our presentation of the rate of separation between the spacecraft, we define the baseline rate in this paper as the sum of the time rate of change of the distance between each collector spacecraft and the combiner (along their line of sight). This definition allows us to capture any component of the rate caused by out-of-plane motion.

Figures 5 and 6 present the baseline and baseline rate as a function of time over the five-day period. These plots are a reflection of the path implied by Eq. (4) subject to the acceleration profile in Eq. (5). The baseline as a function of time in Fig. 5 is relevant to mission planners determining the time between data collection points (based in part on changes in the baseline). The baseline rate shown in Fig. 6 is important as noted in the Introduction because of the impact that relative motion has on the design of the metrology system, primarily the sampling frequency. The small residual baseline rate at the end of the maneuver (0.06 cm/s) is a result of the J_2 acceleration.

The second reference case illustrates the more general situation where the line of sight from the combiner spacecraft to the astronomical target is not perpendicular to the equatorial plane. For this second reference case, $\phi = 45$ deg, and the initial baseline from Eq. (12) is 14.1 m. The results for this reference case are shown in Figs. 7–11. The paths of the two collector spacecraft are shown in Fig. 7. The "flattening" of the ellipse along the v direction ($\hat{\boldsymbol{j}}$ unit vector) is a direct result of the $\cos\phi$ term appearing in Eq. (2) and illustrates a general feature of DeCou's approach, namely, as $\phi \rightarrow 90$ deg, (smaller declination) the synthetic aperture becomes more elongated approaching a linear path along the u direction ($\hat{\boldsymbol{i}}$ unit vector) as the line of sight to the astronomical source approaches the equatorial plane. In reality, the value of ϕ would be limited to some value less than 90 deg either by the need for increased density of observation points or collision-avoidance restrictions on the spacecraft.

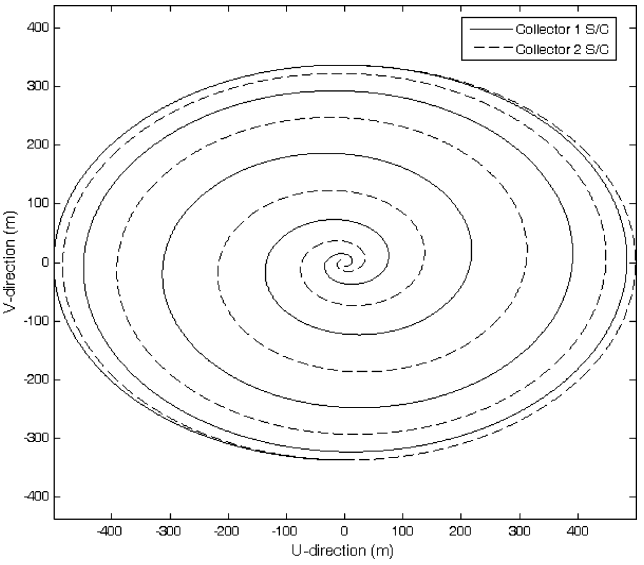

Fig. 7 Path of two collector spacecraft in u–v plane for case corresponding to $D_{\max} = 1000$ m, $\phi = 45$ deg, $\psi = 0$ deg, GEO, and $t_{\text{fill}} =$ five orbits.

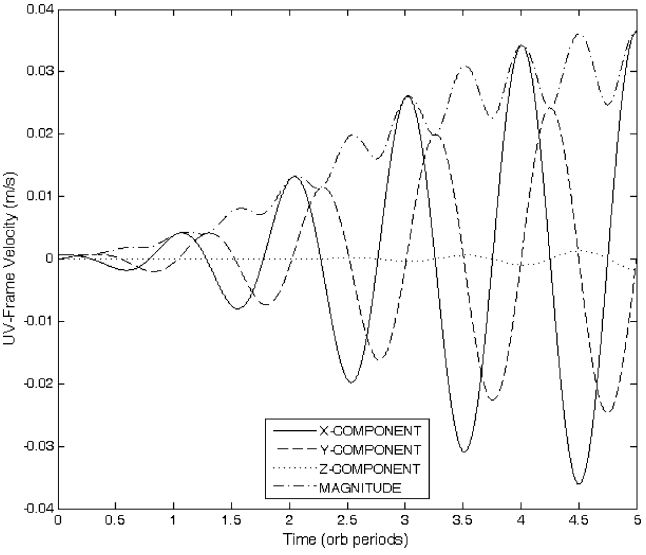

Fig. 8 Velocity components of collector spacecraft in u–v plane for case corresponding to $D_{\max} = 1000$ m, $\phi = 45$ deg, $\psi = 0$ deg, GEO, and $t_{\text{fill}} =$ five orbits.

The velocity and thrust (with no J_2 cancellation) profiles are shown in Figs. 8 and 9. These show a bounding envelope (magnitude), which differs from that in Figs. 3 and 4 also as a result of the $\cos\phi$ term in the acceleration. The maximum thrust for this case, 87 μN, is slightly less than for the first reference case. This additional modulation is further evident in Figs. 10 and 11 for the baseline and baseline rate. The most significant difference is evident in Fig. 11 in which the peak baseline rate of change is seen to increase from a value of 0.48 cm/s for the case depicted in Fig. 6 to 2.4 cm/s for the case in Fig. 11. In addition, the baseline rate oscillates between positive and negative values as the two collectors approach and recede from each other.

These differences are a direct result of the elliptical paths in which the component of the velocity along the baseline increases as $\phi \rightarrow 90$ deg. This rate increase can limit this approach to some range of acceptable target declinations for which the baseline rate of change is within an acceptable limit for a specific metrology system sampling rate. Finally, it is worth noting that the final baseline in

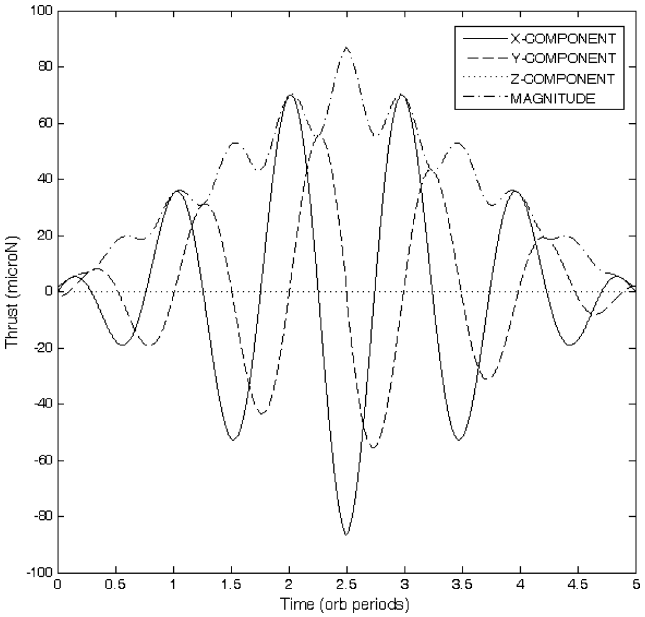

Fig. 9 Thrust components of collector spacecraft in u–v plane for case corresponding to uncompensated J_2 perturbations, $D_{\max} = 1000$ m, $\phi = 45$ deg, $\psi = 0$ deg, GEO, $t_{\text{fill}} =$ five orbits, and $m_{\text{coll}} = 250$ kg.

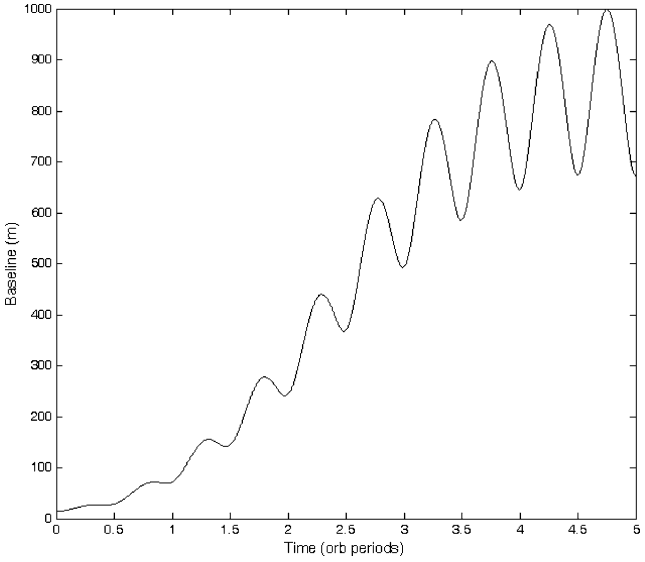

Fig. 10 Formation baseline as a function of time for case corresponding to $D_{\max} = 1000$ m, $\phi = 45$ deg, $\psi = 0$ deg, GEO, and $t_{\text{fill}} =$ five orbits.

Fig. 10 does not correspond to the maximum baseline (as it does for the $\phi = 0$ case in Fig. 5). This is a result of the fact that we have fixed the fill time τ and the baseline does not monotonically increase for the general cases where $\phi \neq 0$.

B. Sensitivity to Altitude, Baseline, and Fill Time

Figures 12–14 present the results of analysis investigating the effect of altitude, maximum baseline, and plane filling time on the maximum required thrust, the maximum baseline rate, and the ΔV to complete the plane filling maneuver. For all of these cases, $\phi = 45$ deg. Two altitudes were considered, geostationary Earth orbit (GEO), corresponding to an altitude of 35,786 km, as in the detailed reference case results, as well as a mid-Earth orbit (MEO), defined for this work to be 20,000-km altitude. In addition to the 1-km maximum baseline considered in the references cases, a smaller 250-m maximum baseline is considered as well. The initial baseline is 14.1 m as before. The orbital elements for the MEO case study are included in Table 1. Finally, a range-of-plane fill time from one to five days was considered.

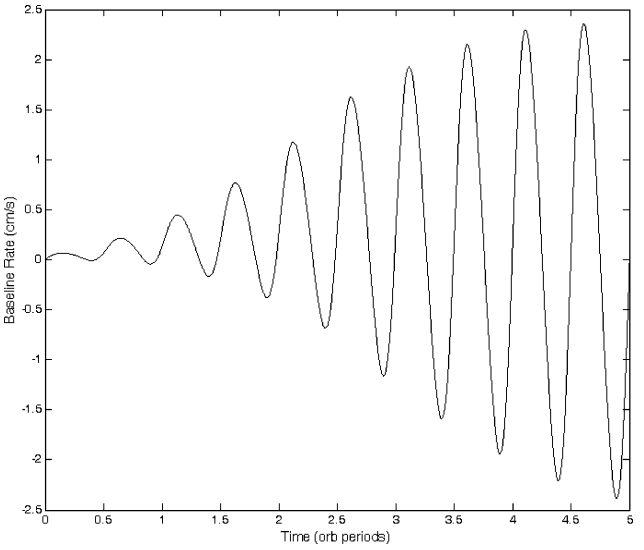

Fig. 11 Formation baseline rate of change as a function of time for case corresponding to $D_{\max} = 1000$ m, $\phi = 45$ deg, $\psi = 0$ deg, GEO, and $t_{\text{fill}} =$ five orbits.

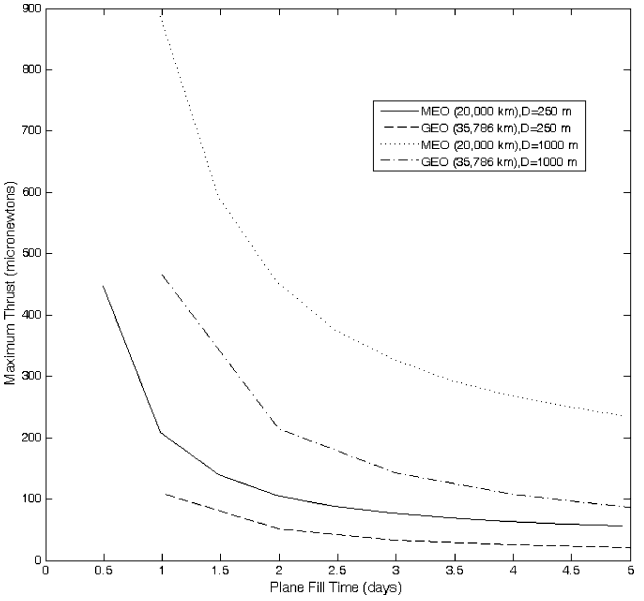

Fig. 12 Maximum required thrust as a function of aperture fill time for cases with $\phi = 45$ deg, $\psi = 0$ deg, and $m_{\text{coll}} = 250$ kg.

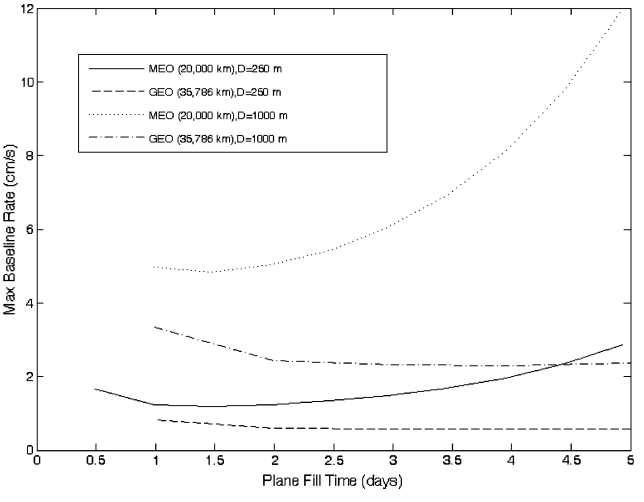

Fig. 13 Formation baseline rate of change as a function of aperture fill time for cases with $\phi = 45$ deg and $\psi = 0$ deg.

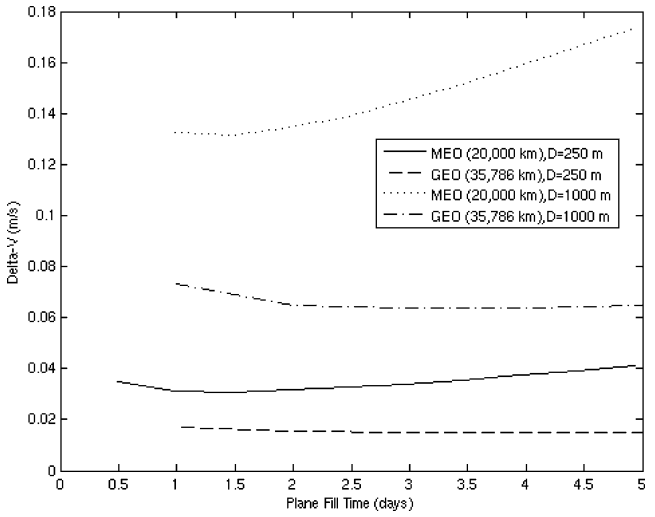

Fig. 14 Required ΔV for aperture filling as a function of aperture fill time for cases with $\phi = 45$ deg and $\psi = 0$ deg.

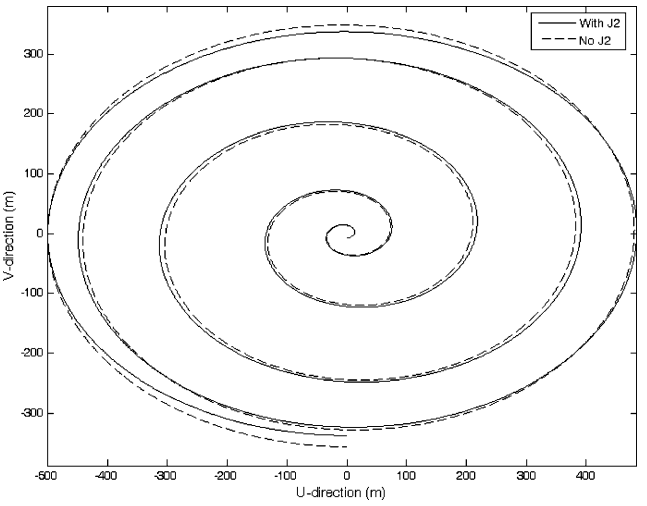

Fig. 15 Path of collector spacecraft (only one shown for clarity) in the u–v plane with and without J_2 perturbing acceleration for case corresponding to $D_{\max} = 1000$ m, $\phi = 45$ deg, $\psi = 0$ deg, GEO, $t_{\text{fill}} =$ five orbits, and $m_{\text{coll}} = 250$ kg.

The thrust plotted in Fig. 12 represents the peak thrust magnitude required for a particular case. This information is useful for the purpose of identifying a candidate thruster technology and estimating propulsion system power requirements. From Fig. 12, one can see that for a given maximum baseline and fill time lowering the altitude increases the peak thrust required [larger ω in Eq. (3)]. For a given altitude and fill time, increasing the maximum baseline increases the required thrust because a larger aperture must be filled in the same amount of time. In all cases, increasing the allocated time to complete the maneuver relaxes the peak thrust requirement. For a 1-km baseline, the benefits of extending the maneuver time diminish beyond four days. For the smaller baseline, the benefits diminish after about two days. The reduction of thrust with extended fill time occurs more gradually for the 1-km baseline because the need for sufficiently high acceleration (and hence thrust) to cover the larger distance in the allocated time is a stronger driver of peak acceleration than the orbital altitude.

From Fig. 13, the maximum baseline rate is seen to be a strong function of fill time for the MEO case and almost insensitive to fill time for the GEO case. As will be discussed in Sec. V, the J_2 acceleration at the lower altitude induces a significant out-of-plane motion. This drift produces the increase in baseline rate with fill time evident for the MEO cases in Fig. 13. At lower altitudes, the orbital frequency is greater, which also leads to a higher baseline rate. Increasing the maximum baseline for a given fill time also increases the relative velocity because a larger distance needs to be covered in the same amount of time.

The ΔV for a given case is the time integral of the thrust acceleration magnitude. The ΔV to complete the plane filling maneuver is seen to be a strong function of the altitude and maximum baseline, but less sensitive to fill time for the GEO case than the MEO case. This trend is also a result of the J_2 acceleration. For the MEO cases, thrust decreases with fill time (Fig. 12) so slowly that there is a net increase in the ΔV with fill time. This trend is almost nonexistent for the GEO cases, in which the out-of-plane motion is much smaller.

C. J_2 Perturbation Effects and Impact on Propulsion Requirements

The results presented in Figs. 2–14 include uncompensated Earth oblateness perturbations (J_2 effects) in the force model. The effect of this perturbation will be a secular change in right ascension of the ascending node and argument of perigee. For a satellite in GEO, this change is approximately -0.01 deg/day in the right ascension of the ascending node and $+0.03$ deg/day in the argument of perigee.[8] The effect that these secular drifts have on formation stability is the focus of numerous studies, including Ref. 9. In the present work, we begin by noting that the formation under consideration is intended for imaging of astronomical rather than terrestrial objects. As a result, the relative drift between spacecraft in the formation is more important than the drift of the formation relative to a specific ground site. In fact, for the MEO case considered (20,000 km), it has been assumed that the formation would be supported by multiple ground stations. In the discussion that follows, we consider the J_2 effect on the formation and then evaluate the thrust required to perform the plane filling maneuvers while canceling the perturbing acceleration. We recall that the origin of the ijk coordinate system coincides with the combiner spacecraft. As such, it is useful to divide the induced drift between a collector and the combiner spacecraft resulting from the J_2 perturbation into components lying in the u–v plane and those perpendicular to it. We will show that the out-of-plane movement has more serious implications in terms of how the mission is designed.

For the first reference case considered earlier ($\phi = 0$ deg; Figs. 2–6), the u–v plane lies in the Earth's equatorial plane. For this case, there is no z component of position in either reference frame. From Eq. (12) we see that the z component of the J_2 acceleration will also be equal to zero, and as a result the J_2-induced drift is limited to the u–v plane. For the more general case with $\phi \neq 0$, there will be an out-of-plane component of acceleration as well. In Fig. 15 we have plotted the path of a collector spacecraft in the u–v plane for the second reference case ($\phi = 45$ deg; Figs. 7–11) with and without the J_2 acceleration included. This is the same case presented in Fig. 7 except that for clarity we show the path of one collector only. At the end of the five orbital periods, the difference in position in the u–v plane resulting from the J_2 acceleration is seen to be on the order of several tens of meters. Because the maneuver is intended to produce a reasonably uniform filling of the image plane, an offset in the spiral path as shown in Fig. 15 will not have a significant impact on the density of observation points. The movement out of plane has more serious implications, however.

In Fig. 16 we plot the out-of-plane z component of the displacement for a single collector spacecraft corresponding again to the second reference case that was shown in Fig. 15. With no J_2 acceleration, the out-of-plane displacement is less than a meter, confirming the correctness of the thrust profile prescribed by DeCou for the case with no perturbation. The curve corresponding to the solution in which J_2 acceleration has been included is seen to develop significant out-of-plane motion over the five orbital periods. The second collector spacecraft has a similar out-of-plane motion but of opposite sign. The result is a "tilting" of the plane defined by the three spacecraft relative to the u–v plane.

The u–v plane is perpendicular to the line of sight to the object being observed. Ideally, the collector spacecraft should lie on the u–v plane so that a wave front of light from the star or other object will reach the collectors at the same time. In actuality, small path differences can be compensated for with a delay line within the

Table 2 Summary of propulsion requirements for one- and five-day fill times with and without compensation for Earth oblateness perturbations

			Without J_2 compensation		With J_2 compensation	
Combiner orbit (altitude, km)	Baseline, km	Fill time, days	T_{max}, μN	ΔV, m/s	T_{max}, mN	ΔV, m/s
MEO (20,000)	250	1	204.7	0.031	13.74	4.72
		5	55.4	0.041	13.63	23.52
MEO (20,000)	1000	1	875.6	0.132	14.22	4.81
		5	234.6	0.174	13.72	23.60
GEO (35,786)	250	1	109.1	0.017	2.16	0.73
		5	20.3	0.015	2.10	3.60
GEO (35,786)	1000	1	463.9	0.073	2.43	0.78
		5	86.6	0.064	2.14	3.64

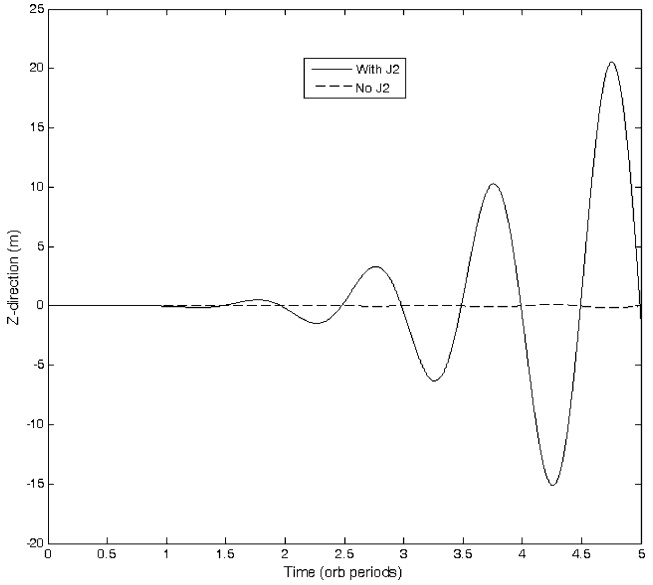

Fig. 16 Component of displacement out of *u–v* plane for single collector with and without J_2 perturbing acceleration for case corresponding to $D_{max} = 1000$ m, $\phi = 45$ deg, $\psi = 0$ deg, GEO, t_{fill} = five orbits, and $m_{coll} = 250$ kg.

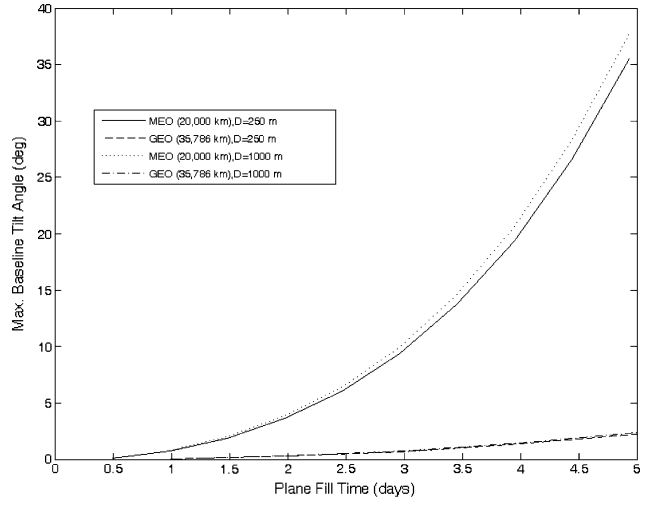

Fig. 17 Maximum baseline tilt angle (out of the *u–v* plane) as a function of aperture fill time for cases with $\phi = 45$ deg and $\psi = 0$ deg.

combiner optical assembly. The acceptable magnitude of this path difference will be instrument specific and is beyond the scope of the present study.

The maximum out-of-plane tilt angle for the cases considered in Figs. 12–14 is shown in Fig. 17 from which we can make the following observations. First, the degradation of the formation as a result of the out-of-plane acceleration is very sensitive to altitude as one might expect, and implementation of the formation at the

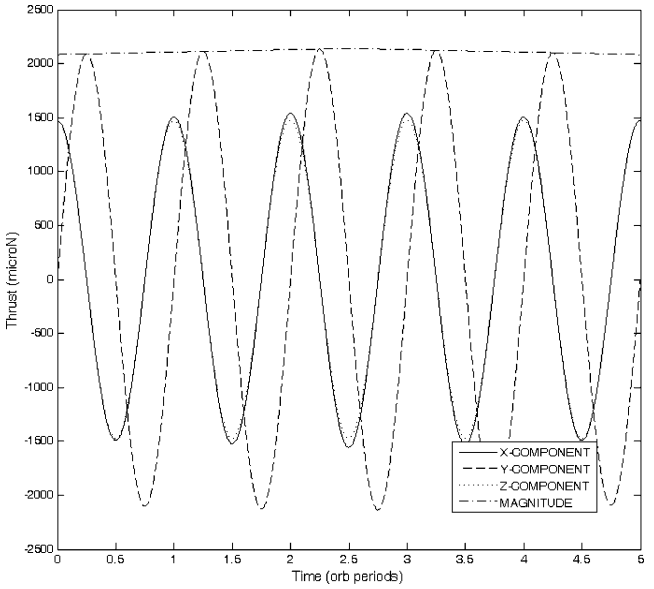

Fig. 18 Thrust components (including cancellation of J_2 perturbing acceleration) for collector spacecraft in *u–v* plane for case corresponding to $D_{max} = 1000$ m, $\phi = 45$ deg, $\psi = 0$ deg, GEO, t_{fill} = five orbits, and $m_{coll} = 250$ kg.

MEO orbit considered is likely infeasible unless the J_2 acceleration can be cancelled by thrusting as will be described next. The second observation is that at GEO the implementation of the formation (without J_2 cancellation) with a fill time of four to five orbital periods (to keep the required thrust below 100 μN) would require that the delay line be able to accommodate an out-of-plane tilt angle on the order of 2 deg. This corresponds to an optical path length mismatch of 1000 tan(2 deg) = 35 m for the 1000-m baseline and 8.7 m for the 250-m baseline. An alternative to imposing such a demand on the instrument is to require the thrusters to effectively cancel the J_2 acceleration.

To determine the thrust required to complete the plane filling maneuver while canceling the effect of the J_2 perturbation, the acceleration components given by Eq. (12) were transformed into the *ijk* coordinate system and added (opposite in sign) to the prescribed thrust profile for plane filling. This result is shown in Fig. 18 for the second reference case. Comparing Fig. 18 with Fig. 9 (same case but without the J_2 cancellation), we see the thrust level is still modulated on a timescale corresponding to the orbital period, but the maximum thrust required is now 2.14 mN with a corresponding ΔV of 3.6 m/s. Another difference is the presence of a z component of thrust, absent from Fig. 9, which arises from the J_2 cancellation. The resulting propulsion requirements for both compensated and uncompensated J_2 effects corresponding to fill times of one and five days are summarized in Table 2.

V. Propulsion Options

The following subsections describe three thruster candidate technologies: pulsed plasma, field emission, and colloid, which we

Table 3 Performance characteristics for selected thruster options

Parameter	PPT[2]	Cs-FEEP[9]	In-FEEP[9]	Colloid[9]
I_{sp}, s	1,150	6,000–12,000	4,000–11,000	500–1,500
T/P, μN/W[a]	18	17	15	20

[a]Depending on the design, the T/P for the FEEP and colloid thrusters could be slightly lower because of the power required for heaters and neutralizer.

believe are enabling for an Earth-orbiting interferometer as considered here. For a detailed description of the thruster physics and detailed performance characteristics, the reader is referred to the references cited and the references therein. Representative values of thrust-to-power ratio and specific impulse are listed in Table 3. Although there is no "magic" maximum allowable thrust level, we treat 100 μN as a benchmark because the field emission and colloid thrusters described next are under development for flight validation at a thrust level of up to 30 μN and could easily be scaled up to 100 μN by using additional units.

A. Pulsed Plasma Thruster

The ablative pulsed plasma thruster was considered as a candidate for the Deep Space 3 distributed spacecraft interferometer mission[2] in part because of its ability to precisely vary thrust level. This device represents a class of solid (Teflon®) fueled pulsed plasma thrusters, which ablate a solid Teflon surface, ionizing and accelerating the resulting plasma to high velocity through a combination of electromagnetic and electrothermal mechanisms.[10–13] Thrust control is achieved through adjustment of the capacitor charging voltage and hence stored energy (which controls the impulse bit for a single pulse) and the pulse repetition frequency (which determines the thrust level for a given impulse bit per pulse). For example, the study in Ref. 2 assumed a 50-μN-s minimum impulse bit achievable with a 5-J charge on the capacitor. To achieve a 10-μN thrust level would therefore require a 0.2-Hz pulse repetition frequency. If finer control is needed, alternative pulsed plasma thrusters, which can achieve smaller impulse bits and more precise control, have been investigated. The U.S. Air Force Research Laboratory MicroPPT[14] was designed for use on small (25-kg) microsatellites with a minimum impulse bit closer to 10 μN-s. Even smaller impulse bits can be achieved with a gas-fed PPT (GF-PPT) such as the one considered for the Terrestrial Planet Finder.[15] With a GF-PPT however, one loses much of the system benefits of a solid propellant as with the ablative Teflon-fueled PPT or the liquid propellant of the remaining systems considered.

The ablative PPT is the most mature of the three propulsion technologies considered, and previous work has considered plume contamination and its effects.[12,13] A PPT built by Aerojet (Redmond, Washington) was one of the technologies successfully demonstrated on NASA's EO-1 spacecraft. For this PPT, a representative operating point is an impulse bit of 0.7 mN-s at a pulse energy of 40 J. Under these conditions, operating at a pulse repetition frequency of 3 Hz, an EO-1 like thruster could produce a thrust of 2.1 mN.

B. Field Emission Electric Propulsion

Field-emission electric-propulsion (FEEP) thrusters are currently under development in Europe for possible use on the LISA mission.[16] These devices rely on the field emission of ions from a liquid metal surface, which is subject to a strong electric field. These are electrostatic thrusters, which require use of a separate neutralizer cathode in addition to a heater to ensure the propellant remains in a liquid state. ALTA/Centrospazio is developing a thruster that uses cesium as the propellant (melting point 28°C),[16,17] and the Austrian Research Center Seibersdorf is developing a thruster that uses indium as the propellant (melting point 150°C).[16,18] Both of these FEEP variants use propellants that are solid at room temperature and heated to a liquid state during operation. While imposing a modest power penalty (heater and neutralizer cathode power is included in the thrust-to-power ratio listed in Table 3), the solid-liquid propellant results in a compact device. The cesium FEEP uses a slit geometry in which multiple emitting sites are established along the fluid surface exposed to the electric field. The indium FEEP uses single needle emitters (which can be formed into an array) that have a single emitting site at the tip. Both the cesium and indium FEEPs rely on capillary action rather than a pressurized feed system to replenish the propellant removed through emission. Besides the difference in melting points, cesium and indium have vapor pressures that differ by many orders of magnitude (10^{-6} torr at 28°C for Cs vs 10^{-19} torr at 150°C for In) resulting in a lower evaporation rate (and contamination risk) for the latter. This difference in the vapor pressure has implications with regard to contamination risk to spacecraft surfaces. The desired operating mode for a FEEP thruster is one in which emission consists of purely ions and no droplets. Ion emission accounts for the high-specific-impulse characteristic of these devices as listed in Table 3. For a given emitter slit length (for the Cs FEEP) or for the number of needles (for the In FEEP), increases in thrust are achieved electrically through changes in the emission current and/or changes in the kinetic energy of the accelerated ion. Increasing the exhaust velocity (specific impulse) might undesirably increase the required accelerating voltage, and so increasing thrust is accomplished through increasing the emission current. This however also has limitations because the emission of droplets and lower mass utilization efficiency will result if one attempts to extract too much current from a single emitter. Therefore, achieving a thrust on the order of millinewtons would require a careful consideration of the range of efficient operation, which can be achieved through beam current and the number of needles (or length of emission slit) needed to achieve the maximum thrust level required.

C. Colloid Thruster

Colloid thrusters rely on feeding a conductive liquid through a metal or coated silica capillary (inner diameter of 30–100 μm) with the exposed fluid at the tip being subjected to an electric field. The electric field creates stresses on the fluid surface, which under certain conditions will assume a conical shape at the surface (Taylor cone) along with the formation of a fluid jet at the apex of this cone. The correct conditions for the formation of a stable electrospray involve balance of the fluid hydrodynamic forces and electrostatic forces on the surface. Conditions for stable operation will depend on the applied electric field as well as the fluid flow rate and conductivity. Unlike FEEP thrusters, which are designed to emit primarily ions, colloid thrusters were originally developed to emit charged droplets of a conductive liquid. Sufficiently high conductivity can allow one to operate primarily in an ion emission regime with an increase in specific impulse and lowering of the thrust-to-power ratio.

Colloid thrusters are also under consideration for the LISA mission and are being developed by Busek Co., Inc. (Natick, Massachusetts), for the ST-7 mission, which will demonstrate key technologies for future so-called drag free missions.[16,19] The colloid performance data listed in Table 3 are based on the colloid micronewton thruster (CMNT) under development for ST-7, which uses a pure ionic liquid (EMI-Im) with a melting point of −55°C as the propellant.[16] A significant difference between the colloid and FEEP thrusters as relates to this work is the fact that the colloid thruster uses a pressure-driven propellant feed system. As a result, thrust can be changed both through electrical and mechanical means. The voltage on an accelerating electrode can be used for minor adjustments to the thrust over short timescales (<100 ms), whereas large changes over longer timescales can be accomplished through flow rate changes.[16] The CMNT uses a constant-pressure, bellows feed with flow controlled by a piezoactuated microvalve to achieve better than 1-nA current resolution (per needle).[16] The combination of electrical and flow control achievable with the colloid thruster provides a large measure of flexibility in the design of a system for any specific mission. As with the FEEP thrusters, multiple needles can be assembled into an array to achieve thrust levels in the millinewton range.

VI. Suitability of Propulsion Options

The three thruster technologies discussed in Sec. V were selected in large part based on their ability to provide precise controllability of thrust level. We can now summarize the propulsion requirements

(Table 2) on the basis of our results from the second, more general, reference case.

The thrust level is the product of the thrust acceleration and the collector spacecraft mass. As noted in the Introduction, the assumed mass of 250 kg is consistent with estimates of mass from a previous study.[2] From Figs. 4 and 9 it is evident that the thrust modulation has two drivers. The first is the modulation with a period equal to the orbital period evident in the thrust components. This is a direct result of the required thrust acceleration vector rotating in the u–v plane. The second driver is the linear increase (and subsequent decrease) in the thrust magnitude, which results from the need to accelerate and then decelerate to form the spiral path for the plane filling maneuver.

If one assumes that thrusters (or thruster clusters) are mounted on the spacecraft such that the thrust vector orientation is fixed with respect to a spacecraft coordinate system, then the required thrust profile, shown in Fig. 4, could be achieved by having the magnitude of the $\hat{\boldsymbol{i}}$ and $\hat{\boldsymbol{j}}$ thrust components increase and decrease while rotating the spacecraft with an angular rate equal to the orbital frequency. The combiner spacecraft, centrally located between the two collector spacecraft, would also rotate at this frequency (about the observation line of sight in the $\hat{\boldsymbol{k}}$ direction) so as to maintain pointing of the instruments with respect to the object and the two collectors.

Assuming that the thrusters are fixed on, and rotating with, the spacecraft, the throttling rate is found from Fig. 9 to be approximately 0.24 μN/min with a corresponding peak thrust of 87 μN as noted earlier. If we require that the thrusters cancel the J_2 acceleration components, the throttling rate is found from Fig. 18 to be approximately 5.25 μN/min with a corresponding peak thrust of 2.14 mN. These rates of change are well within the capabilities of any of the three technologies proposed in Sec. II. The thrust level of 2.14 mN would require a scale-up of the colloid or FEEP thrusters under development for ST-7 but should be easily managed with the PPT.

In addition to maximum thrust and throttling rate, two additional propulsion requirements are propellant mass and minimum thruster power. The calculated ΔV for the second reference case are found to be 0.064 m/s (without J_2 cancellation) and 3.6 m/s (with J_2 cancellation). If we assume a total observation ΔV budget of 6.5 m/s (100 objects imaged with no J_2 cancellation), and the lowest specific impulse listed in Table 3 (500 s for colloid), the corresponding propellant mass can be determined from the rocket equation and is found to be 0.33 kg. Including J_2 cancellation, the same 100 objects would require a propellant mass of 17.7 kg at 500-s specific impulse, or 7.9 kg if we assume the 1150-s specific impulse corresponding to the PPT. Additional propellant mass and ΔV would be budgeted for retargeting and other maneuvers, which could be accomplished with the same thrusters or a different system altogether.

Finally we can estimate the thruster power based on the peak thrust required we have calculated for the maneuver. For the thrust-to-power ratios listed in Table 3, the power ranges from 4.4–5.8 W for the three technology options. The corresponding power if J_2 cancellation is included is 107–143 W. These ranges are easily obtained with a solar-array power system.

The requirements summarized here were based on the second reference case. Requirements for the MEO altitude, 250-km baseline, or any fill time between one and five days can be obtained by using the data plotted in Figs. 12 and 14. Other spacecraft masses can also be considered because the thrust results in Fig. 12 scale linearly with spacecraft mass.

An important result of this study is the calculation of the amount of out-of-plane motion resulting from the J_2 perturbation. The effect is a tilting of the plane defined by the three spacecraft relative to the u–v image plane. For a tilt angle of even two degrees, the out-of-plane motion results in a starlight path length mismatch of 35 m for a 1000-m baseline filled over a four to five day period. Such a large mismatch is likely to be unacceptable from the standpoint of interferometer design.

Two solutions are proposed to mitigate this problem. One solution is to complete the maneuver in one day, which results in a maximum out-of-plane motion (sum for both collectors) of 1.1 m. This solution requires a maximum thrust of 464 μN (Fig. 12) and imposes a maximum baseline rate of change of 3.3 cm/s (Fig. 13). A second solution is to use the thrusters to identically cancel the J_2 acceleration. This requires a maximum of 2.14 mN of thrust but allows the maneuver to be completed over a five-day period instead with a maximum baseline rate of change of 2.2 cm/s and a maximum out-of-plane motion of 0.3 m. The thruster technologies described are capable of meeting the thrust level required for either of these solutions. Through a suitable placement of the thrusters and a rotation of the spacecraft at the orbital frequency, much of the modulation can be accomplished by virtue of the fact the thrust vectors rotate with the spacecraft in the imaging plane. The determination of which solution is preferable will likely depend on the detailed design of the instrument rather than the thrusters. The reason for this is that filling the image plane in one day implies a higher velocity for the collectors through the u–v plane, and hence the time available for data collection at any point is reduced. This might be problematic for fainter objects requiring longer acquisition times.

VII. Conclusions

The Earth-orbiting, imaging formation approach developed by DeCou was investigated with the objective of identifying propulsion requirements (specifically the maximum thrust level and modulation rate) including the effect of J_2 perturbations. The analysis was based on a numerical integration of the equations of motion subject to the acceleration profile originally proposed by DeCou and including approximate force model to account for a nonspherical Earth.

Revisiting the five objectives for this study listed in the Introduction, it was found that results from the numerical analysis are consistent with the analytical results from Ref. 3. The calculations show that for spacecraft mass of 250 kg, consistent with interferometer spacecraft estimates from detailed studies of the DS-3 mission, the plane filling maneuver can be achieved with a maximum thrust level less than 100 μN for a formation at GEO, with five days allocated to completing a maneuver corresponding to a maximum baseline of 1000 m. The result of including the J_2 perturbation is to introduce a tilting of the plane defined by the three spacecraft relative to the u–v image plane. As discussed, this has implications for the instrument, and a more demanding set of propulsion requirements were quantified in order to compensate for this effect. The sensitivity of the maximum required thrust ΔV and baseline rate of change to orbital altitude, allocated time for the plane filling maneuver, and maximum interferometer baseline were quantified. Several thruster options, which are potentially enabling for this mission and two strategies to mitigate the plane tilting problem, were described.

The development of thrusters capable of precision control in the micronewton and millinewton thrust range over the last several years has opened the possibility of realizing the plane filling strategy proposed by DeCou in 1991.

Acknowledgment

The authors thank Adam Siegel for his contributions to the early analysis and many valuable discussions.

References

[1]Blackwood, G. H., Dubovitsky, S., Linfield, R. P., and Gorham, P. W., "Interferometer Instrument Design for New Millennium Deep Space 3," Society of Photo-Optical Instrumentation Engineers, Paper 3350-83, March 1998.

[2]Blandino, J. J., and Cassady, R. J., "Propulsion Requirements and Options for the New Millennium Interferometer (DS-3) Mission," AIAA Paper 98-3331, July 1998.

[3]DeCou, A. B., "Orbital Station-Keeping for Multiple Spacecraft Interferometry," *Journal of the Astronautical Sciences*, Vol. 39, No. 3, 1991, pp. 283–297.

[4]DeCou, A. B., "Gravity Gradient Disturbances on Rotating Tethered Systems in Circular Orbit," *Proceedings of the Third International Conference on Tethers in Space*, AIAA, Washington, DC, 1989, pp. 343–351.

[5]Dubovitsky, S., Linfield, R. P., Blackwood, G. H., and Gorham, P. W., "Deep Space 3 Metrology System," Society of Photo-Optical Instrumentation Engineers, Paper 3350-11, March 1998.

[6]Siegel, A., and Blandino, J., "Propulsion Requirements and Options for Astronomical Imaging Formations in Earth Orbit," AIAA Paper 2003-4577, July 2003.

[7]Vallado, D. A., *Fundamentals of Astrodynamics and Applications*, 2nd ed., Space Technology Library, Microcosm Press, El Segundo, CA, and Kluwer Academic, Boston, 2001, p. 551.

[8]Wertz, J. R., and Larson, W. J., *Space Mission Analysis and Design*, 3rd ed., Space Technology Library, Microcosm Press, El Segundo, CA, and Kluwer Academic, Boston, 1999, p. 144.

[9]Sabol, C., Burns, R., and McLaughlin, C. A., "Satellite Formation Flying Design and Evolution," *Journal of Spacecraft and Rockets*, Vol. 38, No. 2, 2001, pp. 270–286.

[10]Cassady, R. J., Willey, M. J., Meckel, N. J., and Blandino, J. J., "Pulsed Plasma Thruster for the New Millennium Space Interferometer Experiment DS-3," AIAA Paper 98-3326, July 1998.

[11]Tilley, D. L., Pobst, J. A., Bromaghim, D. R., Myers, R. M., Cassady, R. J., Hoskins, W. A., Meckel, N. J., Blandino, J. J., Brinza, D. E., and Henry, M. D., "Advanced Pulsed Plasma Thruster Demonstration on MightySat Flight II.1," *Proceedings of the 10th AIAA/Utah State University Conference on Small Satellites*, 1996.

[12]Blandino, J. J., Cassady, R. J, and Peterson, T. T., "Pulsed Plasma Thrusters for the New Millennium Interferometer (DS-3) Mission," International Electric Propulsion Conf., Paper 97-192, Aug. 1997.

[13]Arrington, L. A., Marrese, C. M., and Blandino, J. J., "Pulsed Plasma Thruster Plume Study: Symmetry and Impact on Spacecraft Surfaces," AIAA Paper 2000-3262, July 2000.

[14]Spanjers, G., Bromaghim, D., Lake, J., Dulligan, M., White, D., Schilling, J., Bushman, S., Antonsen, E., Keidar, M., and Boyd, I., "AFRL MicroPPT Development for Small Spacecraft Propulsion," AIAA Paper 2002-3974, July 2002.

[15]Polzin, K. A., Choueiri, E. Y., Gurfil, P., and Kasdin, N. J., "Plasma Propulsion Options for Multiple Terrestrial Planet Finder Architectures," *Journal of Spacecraft and Rockets*, Vol. 39, No. 3, 2002, pp. 347–356.

[16]Ziemer, J. K., and Merkowitz, S. M., "Microthrust Propulsion for the LISA Mission," AIAA Paper 2004-3439, July 2004.

[17]Marcuccio, S., Giannelli, S., and Andrenucci, M., "Attitude and Orbit Control of Small Satellites and Constellations with FEEP Thrusters," International Electric Propulsion Conf., Paper 97-188, Aug. 1997.

[18]Tajmar, M., Genovese, A., and Steiger, W., "Indium Field Emission Electric Propulsion Microthruster Experimental Characterization," *Journal of Propulsion and Power*, Vol. 20, No. 2, 2004, pp. 211–218.

[19]Gamero-Castaño, M., and Hruby, V., "Electrospray as a Source of Nanoparticles for Efficient Colloid Thrusters," AIAA Paper 2000-3265, July 2000.

C. McLaughlin
Associate Editor